

PAPER • OPEN ACCESS

## Self-adaptive multimethod optimization applied to a tailored heating forging process

To cite this article: M Baldan *et al* 2018 *IOP Conf. Ser.: Mater. Sci. Eng.* **355** 012016

View the [article online](#) for updates and enhancements.



**IOP | ebooks™**

Bringing you innovative digital publishing with leading voices to create your essential collection of books in STEM research.

Start exploring the collection - download the first chapter of every title for free.

# Self-adaptive multimethod optimization applied to a tailored heating forging process

M Baldan<sup>1</sup>, T Steinberg<sup>1</sup> and E Baake<sup>1</sup>

<sup>1</sup>Institute of Electrotechnology, Leibniz University Hanover, Wihlelm Busch Straße 4, 30167 Hanover - Germany

baldan@etp.uni-hannover.de

**Abstract.** The presented paper describes an innovative self-adaptive multi-objective optimization code. Investigation goals concern proving the superiority of this code compared to NGSA-II and applying it to an inductor's design case study addressed to a "tailored" heating forging application. The choice of the frequency and the heating time are followed by the determination of the turns number and their positions. Finally, a straightforward optimization is performed in order to minimize energy consumption using "optimal control".

## 1. Introduction

Evolutionary algorithms have been successfully applied in the last few decades for solving optimization and design problems of electromagnetic devices [1]. The goal is to determine values for model parameters that provide the best trade-off in the case of multiple conflicting objects. The combination of the multi-objective optimization procedures with problem-oriented mathematical models allows the development of an effective optimization strategy which can be applied to engineering cases. Since the evaluation of the goal functions requires frequently a FEM model, whose computational cost could be significant, it appears to be crucial to reduce the number of evaluations.

Currently, the non-dominated sorted genetic algorithm (NGSA-II) [2] has received the most attention because of its simplicity and demonstrated superiority over other methods and it has been widely used in the design of electromagnetic devices [3]. Nevertheless, NGSA suffers of some drawbacks when the population and number of iteration must be limited to reduce the time of computation: it can occur, e.g. when the objective functions are evaluated using a numerical method like finite element. Moreover, when the number of individuals in the initial population is limited, the solution sometimes is affected by the choice of the initial population [10]. Particle Swarm Optimization (PSO) [4] is a heuristic search technique that simulates the movement of a flock of birds which aim to find food. The relative simplicity of PSO and the fact that it is a population based technique have made it a natural candidate to be used in design problems [5]. On the other hand, in computational electromagnetics, applications and also modifications of Biogeography-Based Optimization (BBO) are an emerging new field of research [6]. However, it has been proved that it is impossible to develop a single algorithm that is always efficient for a diverse set of optimization problems [7].

Inspired by the work of Vrugt et al. [8], we present an optimization procedure which combines the concepts of simultaneous multimethod search and self-adaptive offspring creation. In the proposed code, contrary to NGSA, PSO and BBO, several mechanisms are together combined for generating offspring. This feature clarifies the meaning of "multi-method" search. The "self-adaptively" comes



from the fact that a certain mechanism is preferred if it's more efficient in generating offspring. We intend to apply this innovative optimum search not only to few benchmark problems but also to a real inductor's design case addressed to tailored heating applications. Tailored heating aims at creating a desired temperature profile inside of the work-piece in order to gain desired material properties and/or to minimize energy consumption of e.g. a forging process. Multi-objective optimization aims to find the best combination of geometrical and electromagnetic parameters to fulfil the goals mentioned before.

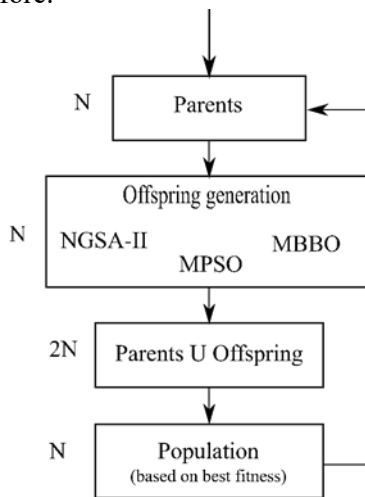


**Figure 1.** Flowchart of the proposed algorithm. The main structure is the same of the NGSA-II code.

## 2. Proposed optimization method

We consider a multi-objective optimization problem, with  $n$  decision variables:  $x = (x_1, \dots, x_n)$  and  $m$  objectives:  $f(x) = (f_1(x), \dots, f_2(x))$  subject to  $g_i(x) \leq 0 \quad i = 1, 2, \dots, r$  and  $h_i(x) = 0 \quad i = 1, 2, \dots, s$ . The presence of multiple objectives give rise to a set of Pareto-optimal solutions, instead of a single solution. A Pareto-optimal solution is one in which one objective cannot be further improved without causing a simultaneous degradation in at least one other objective.

The algorithm here used is a modification of the algorithm AMALGAM proposed by Vrugt et al. [8]. We'll call it, for the sake of simplicity, AMALGAM\*. In Figure 1 is shown the main procedure of the optimization code. The algorithm is initialized by using a random population  $P_0$  of size  $N$ . Then, to each parent is assigned a fitness value based on the non-dominated sorting mode [2]. The population of offspring  $Q_0 = \{Q_0^1, \dots, Q_0^k\}$ , is implemented using  $k$  individual algorithms instead of using a single operator. The chance that one offspring is generated by the  $k$ -th algorithm is proportional to the "specific probability"  $k$ -th of the algorithm itself. If at the beginning each algorithm has the same "specific probability", at each generation, the values are updated according to the success that algorithms have in producing offspring. The idea of using the "specific probability" is an original contribution of the authors. After offspring's creation, a combined population  $R_0 = P_0 \cup Q_0$  of size  $2N$  is created and ranked using the non-dominated sorting mode. The  $N$  members for the next population are chosen according to the rank and the crowding distance of the  $2N$  elements of  $R_0$ . The new population  $P_1$  is then used to create offspring using the already described procedure. This step algorithm is repeated until convergence is reached.

If the vector  $S_t^1, \dots, S_t^k$  indicates the "specific probability" at  $t$  generation,  $\{N_{t-1}^1, \dots, N_{t-1}^k\}$  is the number of offspring that, at the previous generation, each algorithm generated and,  $\{P_t^1, \dots, P_t^k\}$  stands for the number of offspring, produced by the  $k$ -th algorithm, which appear in the current population, the "specific probability" has been calculated as follows (1):

$$S_i^t = \left( \frac{P_t^i}{N_{t-1}^i} \right) \left( \sum_{j=1}^k \frac{P_t^j}{N_{t-1}^j} \right)^{-1} \quad (1)$$

In order to avoid inactivating algorithms, the minimum “specific probability” value was set to 0.1. In AMALGAM\*, we adopted three different algorithms for generation offspring: Non dominated sorting genetic algorithm NSGA-II [2], Multi-objective particle swarm optimization MPSO [4], Multi-objective biogeography-based optimization MBBO [6,9].

NSGA-II uses simulated binary crossover (SBX) and polynomial mutation to create offspring. In the case of MPSO, let  $x_h(t)$  denote the position of the  $h$ -th particle at the iteration  $t$ , the position of the particle is changed by adding a velocity  $v_h(t)$  to the current position (2):

$$x_h(t) = x_h(t-1) + v_h(t) \quad (2)$$

The velocity vector reflects the socially exchanged information. In the case of MPSO, since there is not – like in the single objective case – a best solution, the “best” particle is a random one extracted from an external archive which contains the best  $\lfloor \exp^{2m} \rfloor$  non-dominated particles (particles are sorted by rank and crowding distance). The best particle’s position ever is instead updated when the particle is dominated or if both are incomparable (they are both non-dominated with respect to each other). In MBBO each solution considered is treated as habitat. The offspring are generated by means of two stochastic operators: migration and mutation. Migration is supposed to improve “bad” habitats (which have bad fitness) by sharing features from “good” habitats. Mutation modifies some randomly selected habitats in view of a better exploration of the design space.

In case of constrained optimization, if an offspring (particle) violates one or more constraints in the design space, objective functions are not evaluated. What is calculated is the “violation” (3):

$$vio_h = \sum_{q=1}^r \max(0, g_q(x)) + \sum_{q=1}^s |h_q(x)| \quad (3)$$

Each feasible solution has a better fitness than every other unfeasible solution. Unfeasible solutions are ranked on the basis of their  $vio_h$ : the smaller  $vio_h$ , the better the fitness.

### 3. Numerical test

In this section we intend to test AMALGAM\* applying it to four analytical cases. We adopt the metrics used in [10] to quantify the performance of the proposed algorithm. We evaluate the error between the approximated and exact one, both in the Pareto front (objective function space) and its correspondent inverse image (variable space). Considering  $N_{fr}$  individuals with the lowest rank final front, the geometric distance between each  $h$ -th point  $x = (x_1, \dots, x_n)$  and its inverse image is (4):

$$d_{x,h} = \sqrt{\sum_{i=2}^n (x_{i,h} - f_i^{-1}(x_{1,h}, \dots, x_{n,h}))^2} \quad (4)$$

Where  $f_i^{-1}$  is the  $i$ -th component of the inverse image of the Pareto front. While, in order to evaluate the error in the objective space, in the case of two objective functions (5):

$$d_{f,h} = |f_{2,k} - f_{2,k}(f_{1,k})| \quad (5)$$

With  $f_{2,k}$  is given the exact expression of the Pareto front. The rms error value of the  $N_{fr}$  distances is evaluated in order to compare the performances.

The so called “relative” crowding distance has been also calculated for both the objective and variable spaces. The average “relative” distance of  $N_{fr}$  individuals in the variable space is (6):

$$\sigma_x = \frac{1}{N_{fr} - 1} \sqrt{\sum_{i=1}^n \left[ \frac{\max(x_i) - \min(x_i)}{\max(x_i) - \min(x_i)} \right]^2} = \frac{\sqrt{n}}{N_{fr} - 1} \quad (6)$$

An analogous expression is used in the objective space, where  $n$  is substituted with  $m$  (the space's dimension). The average relative distance is called here  $\sigma_f$ . In the variables space, the relative distance between the  $h$ -th and the  $j$ -th individuals, both in the front, is (7):

$$d_x(h, j) = \sqrt{\sum_{i=1}^n \left[ \frac{x_{h,i} - x_{j,i}}{\max(x_i) - \min(x_i)} \right]^2} \quad h \neq j \quad (7)$$

Again, for the objective space, it's just sufficient to substitute  $n$  with  $m$  and  $x$  with  $f$ . The crowding of the front in terms of design variables  $cw_x(h)$  is the number of individuals,  $j$ -th, which are closer to the individual  $h$ -th than the threshold  $\sigma_x$  (8):

$$cw_x(h) = \sum_{j=1}^{N_{fr}} U_{h,j} \quad \text{with } U_{h,j} = \begin{cases} 1 & \text{if } d_x(h, j) < \sigma_x \\ 0 & \text{if } d_x(h, j) \geq \sigma_x \end{cases} \quad (8)$$

Also here there is a correspondent definition for the objective space.

### 3.1. Test functions

We considered four unconstrained test functions [2,10,11] which are summarized in Table 1.

**Table 1.** Test functions: T1 (A), F2 (B), ZDT1 (C), ZDT2 (D).

n	Variable bounds	Objective functions	Optimal solutions	Pareto front
<b>A</b> 2	[0,2]	$f_1 = x_1^2 + x_2^2$ $f_2 = (x_1 - 1)^2 + (x_2 - 1)^2$	$x_1 = x_2$	$f_2 = f_1 - 2\sqrt{2f_1} + 2$
<b>B</b> 3	$x_1 \in [0,1]$ $x_2, x_3 \in [-1,1]$	$f_1 = x_1 + \frac{2}{3}[x_3 - \sin(6\pi x_1 + \pi)]^2$ $f_2 = 1 - \sqrt{x_1} + \left[x_2 - \sin\left(6\pi x_1 + \frac{2}{3}\pi\right)\right]^2$	$x_i = \sin\left(6\pi x_1 + \frac{i\pi}{n}\right)$ $i = 2, \dots, n$	$f_2 = 1 - \sqrt{f_1}$
<b>C</b> 30	[0,1]	$f_1 = x_1$ $f_2 = g(x)[1 - \sqrt{x_1/g(x)}]$ $g(x) = 1 + 9(\sum_{i=2}^n x_i)/(n-1)$	$x_i = 0$ $i = 2, \dots, n$	$f_2 = 1 - \sqrt{f_1}$
<b>D</b> 10	$x_1 \in [0,1]$ $x_i \in [-5,5],$ $i \neq 1$	$f_1 = x_1$ $f_2 = g(x)[1 - \sqrt{x_1/g(x)}]$ $g(x) = 1 + 10(n-1)$ $+ \sum_{i=2}^n [x_i^2 - 10\cos(4\pi x_i)]$	$x_i = 0$ $i = 2, \dots, n$	$f_2 = 1 - \sqrt{f_1}$

Tests were performed with 20 different starting populations. Here we present the average (over the 20 cases) rms error in both variable and objective spaces, as the most representative indicator in the ability to identify the Pareto front (Table 2). With ‘‘Pop’’ and ‘‘Gen’’ we refer respectively to population's individuals number (called it  $N$  before) and to the generations' number. In other words, we decide a priori the number of calls of the objective functions.

**Table 2.** Comparison of the rms error in the variable and objective space.

Test	Pop	Gen	Code	err <sub>rms</sub> (x)	err <sub>rms</sub> (f)
<b>A</b>	20	20	NGSA-II	0.205	0.068
			AMALGAM*	0.0819	0.0202

<b>A</b>	20	50	NGSA-II	0.125	0.0333
			AMALGAM*	0.0497	0.0118
<b>B</b>	20	50	NGSA-II	0.478	0.332
			AMALGAM*	0.186	0.0511
<b>B</b>	20	100	NGSA-II	0.408	0.3086
			AMALGAM*	0.1377	0.0285
<b>C</b>	100	200	NGSA-II	0.914	0.698
			AMALGAM*	0.0633	0.0398
<b>D</b>	100	300	NGSA-II	**	**
			AMALGAM*	0.4982	0.1838

In every case AMALGAM\* shows an evident superiority compared to NGSA-II. In the case D (\*\*), at every attempt, the code NGSA-II failed the convergence to the real Pareto front. We show here more in details the results in case of test A (Figure 2). A better ability of exploiting the Pareto front is shown by AMALGAM\* compared to NGSA-II. Especially in the left side, results obtained with NGSA-II don't cover the overall extension of the Pareto front. This fact is visible in the calculation of the crowding distance: particles amass much more in the case of NGSA-II (Figure 2).

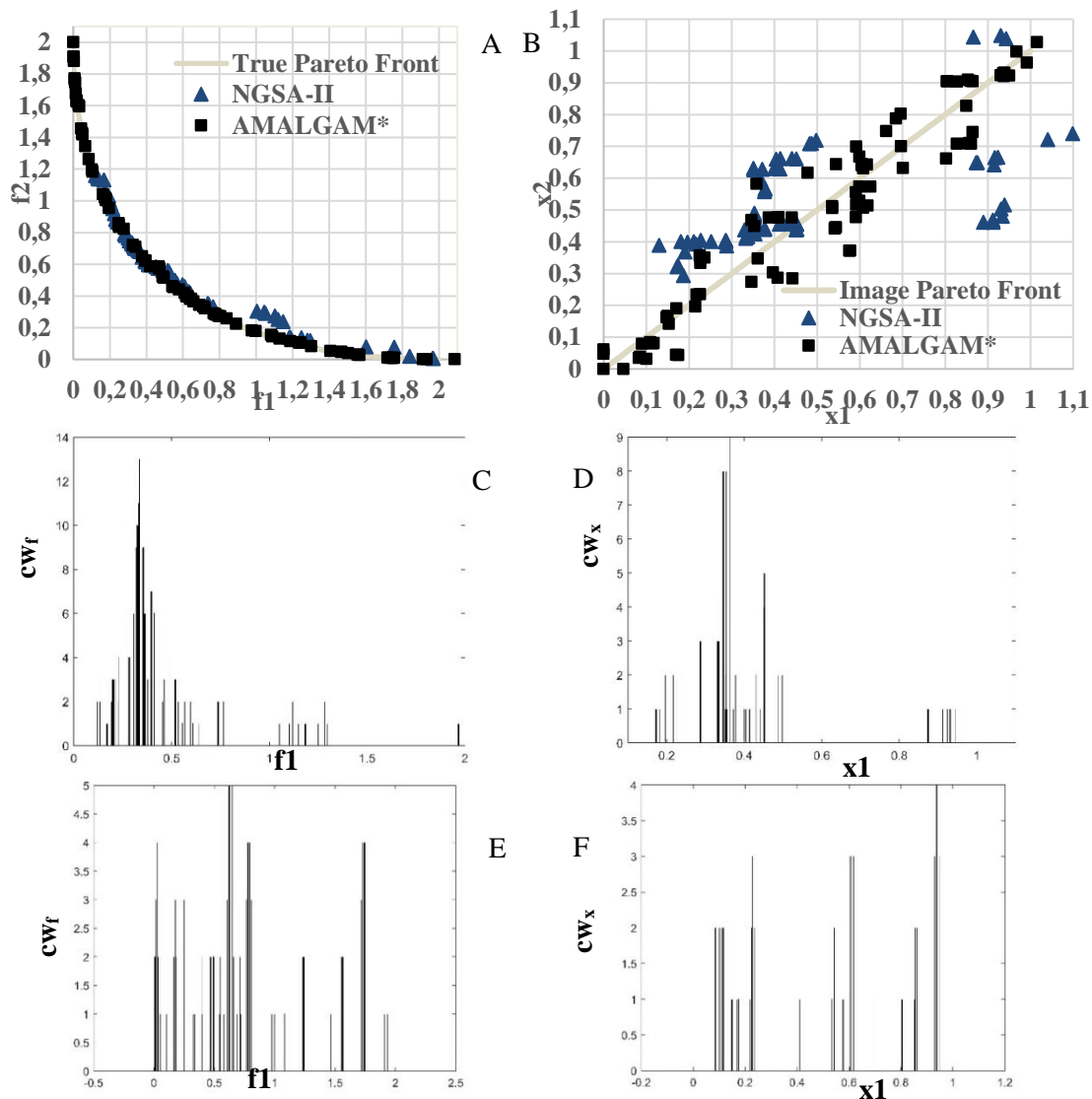


**Figure 2.** Comparison between calculated and true Pareto front in the objective (A) and variable (B) spaces with Pop=20 and Gen=20. Crowding distances in  $f$  and  $x$  spaces with NGSA-II (C-D) and AMALGAM\* (E-F).

#### 4. Tailored heating

In literature the concept of “Tailored heating” refers to an innovative heating approach which is addressed to forging processes [12]. Forging a billet from an initially “simple” geometry to a part of “complex” geometry may require several preform stages. In each stage, a pair of dies must be designed and manufactured. Subsequently, a series of mounting and dismounting die-inserts must be performed in the preform stage. This is often time consuming and costly. Consequently, the die forging of parts with complex geometry is only cost effective for large-batch production. Guo et al. [13] and Kayatürk et al. [14] proposed a thermal differential flat-die forging process, in which the parts of the forging billets which are supposed to have a high material flow are heated up to hot forging temperature. Parts which are supposed not to have such high material flow are at “colder” temperatures like 800-900 °C. This contains the basic idea of “Tailored heating”.

The work-piece under analysis is a 42CrMo4 carbon steel billet with 474 mm length and 30 mm diameter. The problem aims to heat up the billet with a desired temperature profile: two “hot” zones with a uniform temperature of 1200 °C alternate with three “cold” zones which are supposed to reach a uniform temperature of 900 °C. It was considered a coupled electromagnetic-thermal model for the field analysis with the package ANSYS®. The design of an inductor which is able to provide the afore described temperature profile is the topic of this work. It represents a challenging task in which AMALGAM\* has been applied.

##### 4.1. Choice of frequency and heating time

We want to understand which frequency- heating time couple best fits to our purpose. In [12] good results have been reached using a frequency of 4 kHz and a heating time of 70 seconds. We consider for simplicity a 1D model (Figure 3), in which the inductor is a massive piece of copper and the work-piece a 15 mm wide 42CrMo4 body.

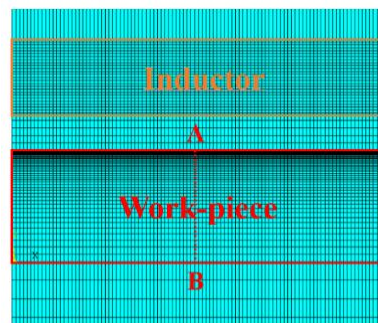


**Figure 3.** 1D model's geometry.

Our intention is to obtain a uniform temperature of 1200 °C. Two objective functions are evaluated: the maximum deviation, at the end of the heating, along the line A-B (see Figure 3) from 1200 °C and the energy consumption (9). A fixed current is applied for the entire duration of the heating.

$$f_1 = \max |T(l_{AB}, t_{heat}) - 1200^\circ|$$

$$f_2 = \int_{t_{heat}} P dt \quad (9)$$

Three design parameters are under investigation: heating time (t), frequency (f) and current (I) (Table 3). Values of current don't have a real physical meaning because we are referring to a 1D model.

**Table 3.** Parameters to be optimized.

t (s)	f (kHz)	I (kA)
40 - 70	4 - 7	4 - 7

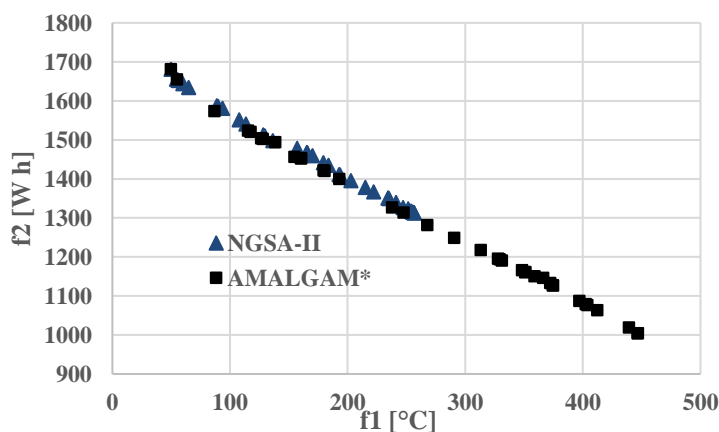


Figure 4 summarizes the results of optimization after 100 generations with a population of 20 individuals. While AMALGAM\* shows a greater ability in exploring the Pareto front compared to the results obtained with NGSa-II, the minimum value of  $f_1$  is practically the same (see Table 4).

**Table 4.** Individual with the minimum value of  $f_1$  (best heating accuracy).

	t (s)	f (kHz)	I (A)	$f_1$ (°C)	$f_2$ (Wh)
<b>NGSA-II</b>	69.8	4	4634	50.9	1682
<b>AMALGAM*</b>	70	4	4626	50.0	1681

As expectable, the maximum homogenization is obtained with longest time and the smallest frequency. What is interesting to see, is that, moving along the Pareto front, with a frequency of 4 kHz and a heating time of 63 s,  $f_1$  values 55°C, which is only 5°C more than the found optimum with minimum  $f_1$ . On the other hand, the energy consumption is in this case 1655 Wh (1.6% less) and the time is drastically reduced. For this reason, we adopt a frequency of 4 kHz and a heating time of 63 s. In Figure 5 instead are shown the trends of the “specific probability” during the 100 generations of the three optimization algorithms used in AMALGAM\*. If at first NGSa-II and MBBO are dominant, the Particle Swarm shows a better ability in exploiting the Pareto front. That’s why it has the maximum specific probability in the last generations.



**Figure 4.** Approximated Pareto front after 100 generations. NGSa-II’s Pareto front is much more limited.

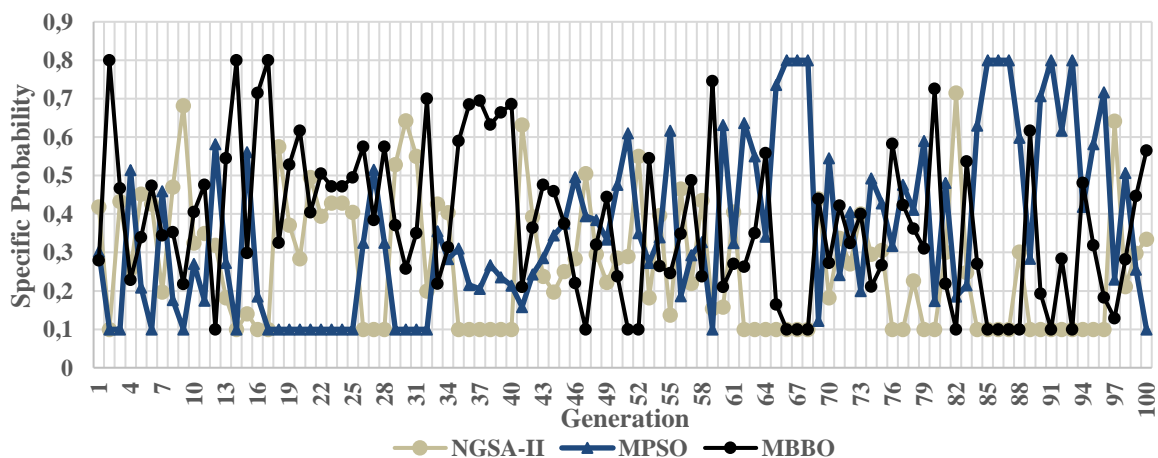


**Figure 5.** Specific probability of NGSa-II, MPSO and MBBO during the 100 generations.



#### 4.2. Inductor's design

The next step is the design of the inductor. Since it's very difficult to define a priori the inductor's configuration (number of turns, air gaps between them...), in the model proposed the inductor is substituted by five nonconductive areas in each of them a uniform current density is applied. In order to speed up the solution, the numerical model consists of one fourth of the system (Figure 6). As design variables, the length  $l_i$  and the current density  $j_i$  applied to each area are considered.  $l_0$  indicates the position of the first area from the middle of the billet. In total 11 variables are under analysis (Table 5).

**Table 5.** Design variables in the inductor's design problem.

$l_0$ (mm)	$l_1$	$l_2$	$l_3$	$l_4$	$l_5$	$j_1$ [A/m <sup>2</sup> ]	$j_2$	$j_3$	$j_4$	$j_5$
1-10	20-60	5-20	70-150	5-40	40-150	0.5-1.0 $10^7$	0.1-0.8 $10^7$	0.8-1.35 $10^7$	0.1-0.9 $10^7$	0.6-1.3 $10^7$

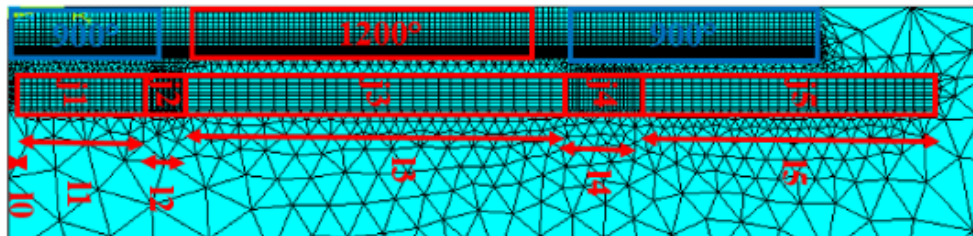


**Figure 6.** Geometry of the model.

The aim is to obtain a uniform temperature of 1200 °C in the hot zone and 900 °C in the cold ones. As visible in Figure 6, we don't take into account the temperature between different zones, in a transition zone 15 mm long. Three objective functions are evaluated (10):

$$\begin{aligned}
 f_1 &= \sum_{i=1}^W |T(x_i, y_i, t_{heat}) - 900^\circ| \\
 f_2 &= \sum_{i=1}^Q |T(x_i, y_i, t_{heat}) - 1200^\circ| \\
 f_3 &= \sum_{i=1}^Z |T(x_i, y_i, t_{heat}) - 900^\circ|
 \end{aligned} \tag{10}$$

Where  $W$  and  $Z$  is the number of nodes respectively in the cold zone at the "centre" and at the "side" of the work-piece.  $Q$  is the number of nodes in the hot zone. Each objective function is the sum of the differences, estimated in each node, between the desired and calculated temperature at the end of the heating. Although this choice doesn't impose any limit to the maximum deviation between final and desired temperature which can be reached in a certain zone, it seems to be more effective in the event that the temperature distribution is only coarsely known. The huge number of variables require a great amount of goal functions' evaluations. A population of 40 individuals after 70 generations has given these results in terms of goal functions (Figure 7).

**Table 6.** Best solution for the inductor's design.

$l_0$ (mm)	$l_1$	$l_2$	$l_3$	$l_4$	$l_5$	$f_1$ (°C)	$f_2$	$f_3$
2.4	20.1	12.9	114.0	18.4	109.5	25.45	65.17	11.45
	$j_1$ (A/m <sup>2</sup> )	$j_2$	$j_3$	$j_4$	$j_5$	$10^3$	$10^3$	$10^3$
	$0.999 \cdot 10^7$	$0.129 \cdot 10^7$	$1.118 \cdot 10^7$	$0.433 \cdot 10^7$	$0.798 \cdot 10^7$			

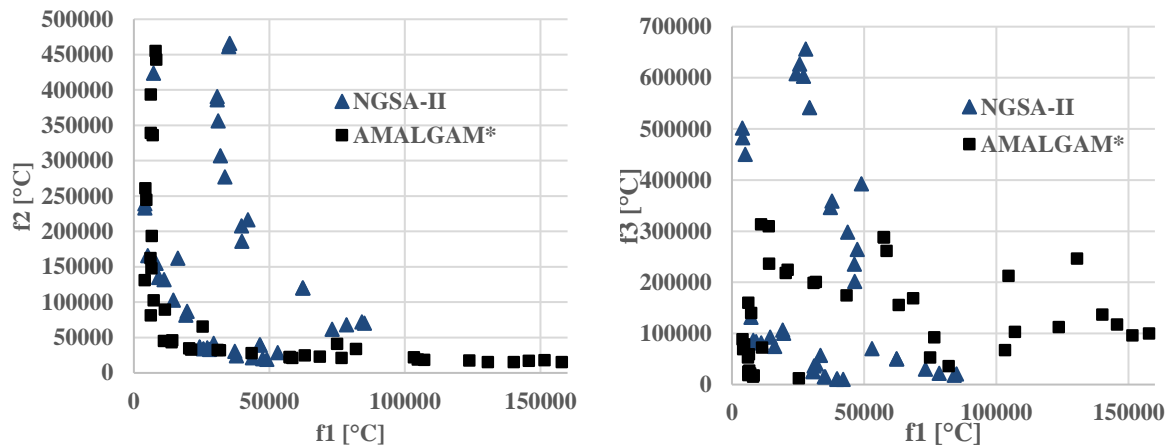


**Figure 7.** Results of optimization after 2800 goal functions evaluations.

For the design of the inductor we consider the closest solution to the “utopia” point (Table 6). From the technological point of view  $f_1$ ,  $f_2$  and  $f_3$  are not fully representative whether the solution is suitable or not. Substantially  $f_2$  with a sum of  $65.17 \cdot 10^3$  keeps a potential to be minimized and thus become

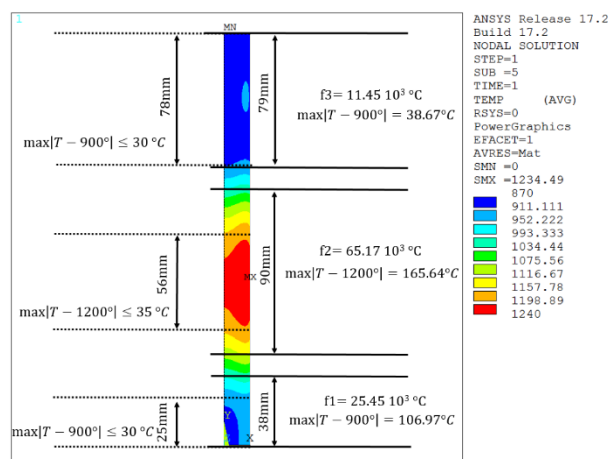


**Figure 8.** Final temperature profile relative to the best solution.

more closely to an optimum solution. In Figure 8 is shown the final temperature distribution relative to the best design point.

Especially in the “hot” zone, the temperature in the whole area is far from being uniform. A quite flat temperature field has been reached only in the middle part of the “hot” zone, instead the maximum deviation from  $1200^\circ\text{C}$  is achieved at the edges. In Table 7 are summarized both the maximum deviations from the goal temperature and the largeness of zone in which the temperature difference doesn’t exceed  $35^\circ\text{C}$ . Referring to the “hot” zone, over a length of 56 mm the temperature doesn’t differ more than  $35^\circ$  from  $1200^\circ\text{C}$ .

**Table 7.** Best solution for the inductor’s design.

	Central “cold” zone	“Hot” zone	External “cold” zone
Length (mm)	38	90	79
Max Deviation ( $^\circ\text{C}$ )	106.97	165.64	38.67
Length (mm)	25	56	78
Max Deviation ( $^\circ\text{C}$ )	< 30	< 35	< 30

### 4.3. Real Inductor

As already done in [12], we need to “translate” this configuration in a real inductor. Each area could be seen as one turn coil. For designing the real inductor, assuming a series connection between turns, it’s possible to convert every one-turn coil in an equivalent multi-turns coil. The total equivalent current (current density times area) which flows in each area is visible in Table 8.

**Table 8.** Total equivalent current.

I1 (A)	I2 (A)	I3 (A)	I4 (A)	I5 (A)
2008	166	12745	797	8738

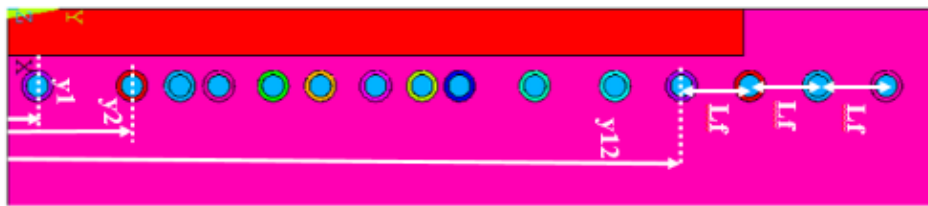


**Figure 9.** Geometry of a generic inductor.

The number of turns in each zone has been chosen as follows: 2 in the first, 7 in the second and 6 in third. In total there are 15 turns in a half inductor, which are equally distributed in each area. The resulting temperature profile is bell-shaped at the centre of the “hot” zone due to the fact that there the magnetic field is maximum. For this reason, a new sub-optimization is performed, in which, the positions of the turns are modified in order to get a more satisfying temperature profile. In this case 13 variables are under analysis: the y positions of the first 12 turns plus the (assumed) constant distance of the last three turns (see Figure 9).

Since the overlapping between turns is not allowed, we’re looking at a constrained optimization case. We set a minimum distance between turn and turn of 1 mm. Using a coil with an external diameter of 10 mm, the following inequalities must be true (11):

$$y_{i+1} - y_i \geq 11 \text{ mm, with } i=1, \dots, 11 \quad (11)$$

In Table 9 the variables’ domains and the solution which best meets our purposes are summarized. Goal functions are the same that have already been used (10). A population of 30 individuals had been run for 100 generations. The total number of evaluations is 2384 for the NGSa-II and 2375 in the case of AMALGAM\*.

**Table 9.** Design parameters and best solution obtained.

	y1	y2	y3	y4	y5	y6	y7	y8	y9	y10	y11	y12	Lf
<b>Min</b>	8.5	38	50	64	80	95	110	127	142	165	190	210	18
<b>Max</b>	12	43	60	74	90	105	125	140	155	180	201	225	26
<b>Best</b>	9.5	40	55.4	68	85.5	100.7	118.5	133.5	144.5	169.8	195.7	217.1	22.0

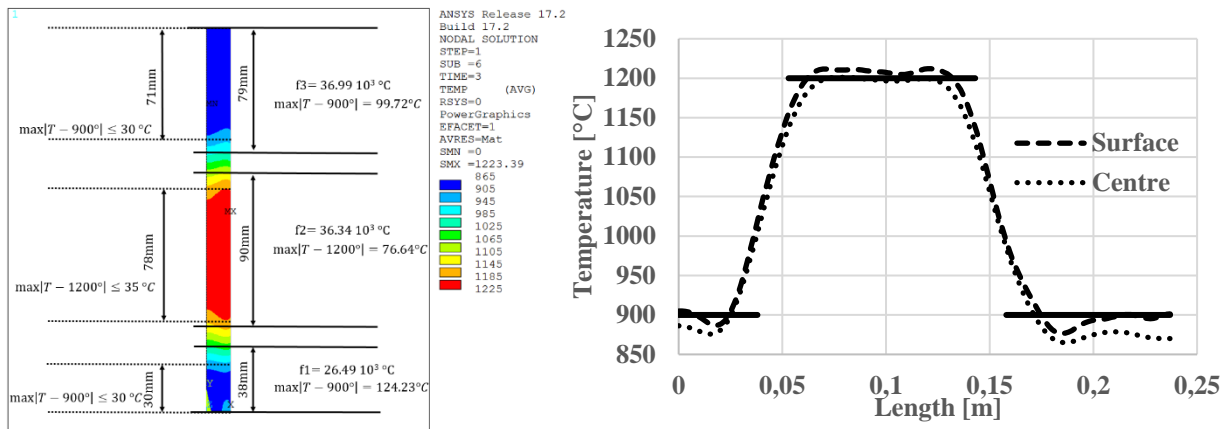


Figure 10. Temperature field (left) at the end of the heating. Temperature profile (right) along the length at the surface and in the centre.

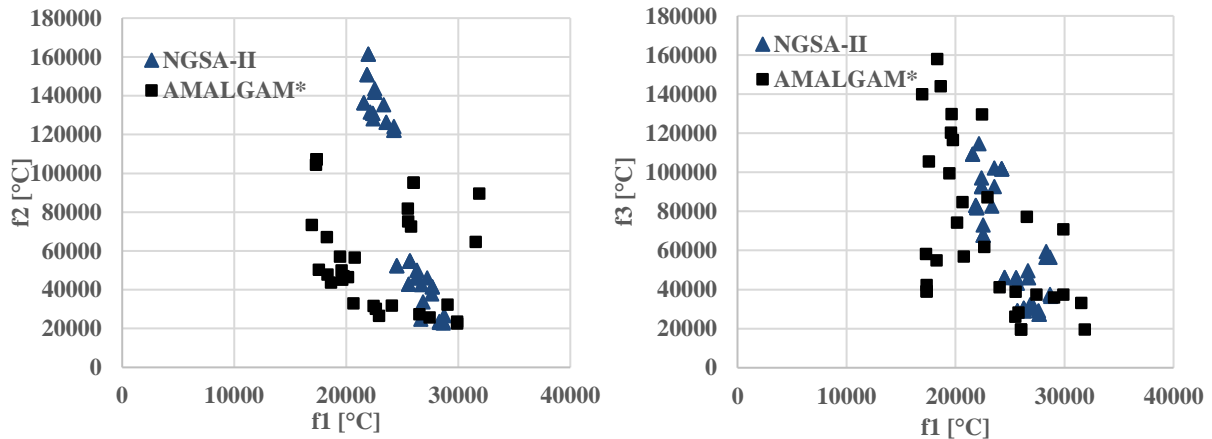


Figure 11. Results of optimization in the real inductor case.

Table 10. Best solution for the inductor’s design.

	Central “cold” zone	“Hot” zone	External “cold” zone
Length (mm)	38	90	79
Max Deviation (°C)	124.23	76.64	99.72
Length (mm)	30	78	71
Max Deviation (°C)	< 30	< 35	< 30

Figure 10 shows the temperature distribution of what is supposed to be the best result from the optimization procedure. A solution with relative small  $f_2$  value is here favourite (Figure 11). Nevertheless, even in the best solution the temperature field diverts considerably from the wished one at the edges of each zone. Table 10 sums up maximum deviations and describes the zones extensions which have a maximum temperature deviation below 35°C. Values are remarkably greater to those in Table 7, which justifies the necessity to perform a sub-optimization. Actually, it has not been found a temperature field in which the “transitions zones” are only 15 mm wide. Transitions in our case study take values of approx. 29 mm, to whose correspond a gradient of 100 °C/cm.

#### 4.4. Optimal control

In this last section we intend to apply the concept of optimal control to the already designed inductor. In general, the ability to control the heating process means a capability to influence a temperature field in order to achieve a desired goal. The temperature distribution can be affected through a set of control inputs. By choosing in every instant the value of each control input, one can modify the temperature distribution and dynamic behaviour of an induction heating system [15]. To choose certain control properly, one needs to determine a cost function, i.e. a function reflecting technical and economic efficiency of system. For example, when maximum productivity is required, a minimal total heating time can be considered as cost function [16].

We intend to reduce the total energy consumption applying a two stage process: in the first the heating under maximum power is performed, in the second no power is provided (soaking period). It is possible to prove mathematically that in case of a static billet which has to be uniformly heated up, time-optimal control consists of alternating stages of heating with maximum power and subsequent soaking. Therefore, the shape of optimal control algorithm is known, but the number of stages and their durations remain unknown. The greater is the number of stages, better is the heating accuracy achievable. In the present work we refer to the simplest case with one heating and one soaking interval, even if it is not proven that this choice is optimal.

Typically, optimal control applications are performed with a defined voltage. That means the heating is characterized by a first interval where the inductor is fed by the maximum voltage available and by a soaking interval. Since in this work we have always thought in terms of current, also in this section we assume the current being the input parameter. In the inductor's optimization a current of 1230 A was given. Supposing we can provide a maximum current of 1500 A – limit given by the maximum power available – we investigated how the energy consumption varies with the heating accuracy.

In summary, the intervals in which vary the two design variables are (Table 11):

**Table 11.** Possible intervals for heating and soaking time.

t <sub>ON</sub> (s)	t <sub>OFF</sub> (s)
30 - 65	0.1 - 15

Goal functions take into account the heating accuracy ( $f_A$ ) and the energy consumption ( $f_B$ ) (13). As in Section 4.2, W, Z and Q are the total number of nodes in the “cold” and “hot” zones.

$$f_A = \sum_{i=1}^W |T(x_i, y_i, t_{heat}) - 900^\circ| + \sum_{i=1}^Q |T(x_i, y_i, t_{heat}) - 1200^\circ| + \sum_{i=1}^Z |T(x_i, y_i, t_{heat}) - 900^\circ|$$

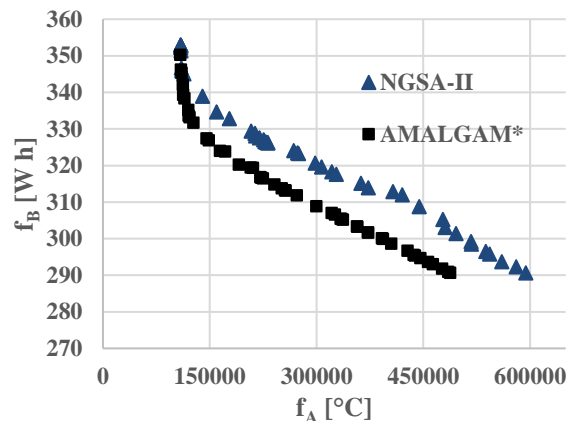
$$f_B = \int_{t_{heat}} P dt \quad (12)$$

Since an excessive overheating of the billet would be not acceptable, a maximum admissible temperature of 1300 °C was set. If during the heating, any point of the billet overcomes 1300 °C, the solution is considered not feasible. Figure 12 shows the Pareto fronts' trend in the case of both, NGS-II and AMALGAM\*, with a population of 30 individuals, after 50 generations.

The estimated Pareto front obtained with AMALGAM\* dominates the NGS-II's one. The best heating accuracy (minimum  $f_A$ ) reached by the two codes is shown in Table 12. In the “normal” heating mode described in the paragraph 4.3,  $f_A$  would value 100671 °C and  $f_B$  355.8 Wh. If on one side the results of optimal control don't bring any improvement in terms of heating accuracy, on the other hand, with a small worsening of the temperature profile, an important reduction of time and energy consumption could be obtained. The soaking time tends indeed to vanish the temperature gradient between zone and zone.

**Table 12.** Minimum value of  $f_A$  in the two codes.

	$t_{ON}$ (s)	$t_{OFF}$ (s)	$f_A$ (°C)	$f_B$ (Wh)
<b>NGSA-II</b>	42.0	6.6	109342	353.0
<b>AMALGAM*</b>	41.4	5.5	108882	350.2

**Figure 12.** Objective functions after 50 generations.

## 5. Conclusions

Using a multimethod optimization search has been found to be a more successful solution in both test and real cases compared to the well-known NGSA-II. Combining different offspring generation methods in a self-adaptive way enables, at each generation, to prevail the most effective ones. In AMALGAM\*, if at first NGSA-II and MBBO hold a high specific probability, when the Pareto front has been identified MPSO remains the most active method. The proposed algorithm improves Pareto front estimation in problems for which objective functions evaluation are computationally expensive. Especially for the tailored heating process, a new inductor design including an optimized set of parameters has been investigated from one benchmark experiment followed by an extensive parameter study. Here it could be shown, that multimethod optimization can be applied successfully in order to minimize the energy consumption by fulfilling the desired temperature profile.

## References

- [1] Di Barba P, Dughiero F, Forzan M and Sieni E 2016 Migration corrected NGSA-II for improving multi-objective design optimization in electromagnetics *Intern. J. of Applied Electromagnetics and Mechanics* **51** 161-72
- [2] Deb K 2002 A fast elitist multi-objective genetic algorithm: NSGA II *IEEE Transaction on evolutionary computation* **6** N. 2 182-97
- [3] Di Barba P, Forzan M and Sieni E 2014 Multi-objective design of a power inductor: a benchmark problem of inverse induction heating *COMPEL The Intern. J. for Computation and Mat.in Electrical and Electronic Engineering* **33** 1990-2005
- [4] Reyes Sierra M and Coello Coello C A 2006 Multi-objective particle swarm optimization: a survey of the state of art *International J. of Computation Intelligence Research* **3** N. 2 287-308
- [5] Nando J and Yahya R S 2008 Particle swarm optimization for antenna designs in engineering electromagnetics *J. of Artificial Evolution and Applications* **2008** 22-10
- [6] Di Barba P, Dughiero F, Mognaschi M E, Savini A and Wiak S 2016 Biogeography-inspired multi-objective optimization and MEMS design *IEEE Transactions on Magnetics* **52** N.3

7201504

- [7] Wolpert D H and Macreasz W G 1997 No free lunch theorems for optimization *IEEE Transactions on evolutionary computations* **1 N.1** 67-82
- [8] Vrugt J Robinson B 2007 Improved evolutionary optimization from generically adaptive multimethod search *PNAS* **104**
- [9] Dan S 2008 Biogeography-based optimization *IEEE Transactions on evolutionary computation* **12 N.6** 702-703
- [10] Sieni E Di Barba P and Forzan M 2016 Migration NGSA: method to improve a non-elitist searching of Pareto front with applications in magnetics *Inverse Problem in Science and Engineering* **24 N. 4** 543-66
- [11] Li H and Zhang Q 2009 Multiobjective optimization problems with complicated Pareto sets, MOEA/D and NGSA-II *IEEE Transactions on evolutionary computation* **13 N. 2** 284-302
- [12] Baldan M Steinberg T and Baake E 2017 Numerical and practical investigation of tailored heating process for forging parts *Proceedings of XVIII UIE Congress* Hannover 338-345
- [13] Guo Y F and Hua M and Osam F H 1997 A preliminary analysis of thermal differential forging – a ring hearer or locally heated cylindrical rod *Proceeding of the 24<sup>th</sup> International Thermal Conductivity Conf. and 12<sup>th</sup> Intern. Thermal Expansion Symposium* Pittsburgh PA 731-45
- [14] Kayatürk K Kurt A Weidig U Steinhoff K Tekkaya A 2001 Simultaneous cold and hot forging in a single forming step – principle, possibilities and limitations *Proceedings of 3th International Conference on Industrial Tools* Slovenia 97-100.
- [15] Rapoport E Pleshivtseva Y 2007 *Optimal Control of Induction Heating Processes* Taylor & Francis
- [16] Pleshivtseva Y Zaikina N Nacke B Nikanorov A Time-optimal control of energy-efficient heating of aluminium billets rotating in DC magnetic field